Available online at www.sciencedirect.com

SCIENCE DIRECT®

PERGAMON

International Journal of Multiphase Flow 29 (2003) 1333–1353

International Journal of Multiphase Flow

www.elsevier.com/locate/ijmulflow

Temperature statistics in particle-laden turbulent homogeneous shear flow

B. Shotorban, F. Mashayek *, R.V.R. Pandya

Department of Mechanical and Industrial Engineering, University of Illinois at Chicago, 842 West Taylor Street, 2053 ERF, Chicago, IL 60607, USA

Received 25 December 2002; received in revised form 25 May 2003

Abstract

Direct numerical simulation is utilized to generate temperature field statistics in particle-laden incompressible homogeneous shear turbulent flows in the presence of mean temperature gradients. The particle density is much larger than the fluid density and the particle volume fraction is small. The particle–particle collisions are ignored, however, both one- and two-way couplings are considered. The effects of the mass loading ratio, the particle time constant, the ratio of specific heats, and the orientation of the mean temperature gradient on the fluid and particle temperature statistics are investigated. The results indicate that the increase of the mass loading ratio or the particle time constant generally tends to decrease the magnitudes of the temperature variance and the turbulent heat flux of both the carrier and the dispersed phases. The increase of the ratio of specific heats increases the particle temperature variance but demonstrates an opposite effect on the fluid. The magnitude of the turbulent heat flux of the fluid is not influenced by the change of the ratio of specific heats whereas that of the particles increases with the increase of this ratio. Further analysis of the results shows that the correlation of the temperature of the particles and the temperature of the fluid at the location of the particles decreases with the increase of the ratio of specific heats or the particle time constant and increases with the increase of the mass loading ratio. The mechanisms responsible for these variations are discussed by examining the budgets of the temperature variance and turbulent heat flux for both phases.

Keywords: Gas–solid flow; Homogeneous shear; Turbulence; Direct numerical simulation; Temperature statistics

* Corresponding author. Tel.: +1-312-996-1154; fax: +1-312-413-0447.
E-mail address: mashayek@uic.edu (F. Mashayek).

0301-9322/03/$ - see front matter
doi:10.1016/S0301-9322(03)00107-1

1. Introduction

Particle-laden turbulent flows have been widely investigated by numerical and experimental methods during the past few decades, however, the complexity of these flows has prevented the formation of a complete mathematical description so far. This is due mainly to the fact that turbulence itself is not fully understood and the presence of particles adds to the complexity of the phenomena involved. Direct numerical simulation (DNS) has been implemented as a reliable tool to accurately study particle-laden flows, however, the need to resolve all scales of turbulence makes DNS applicable mainly in simplified configurations and at low Reynolds numbers. A recent review of DNS studies of two-phase flows in various configurations can be found in Mashayek and Pandya (in press).

Despite its known limitations, DNS has been instrumental in enhancing the physical understanding of many underlying phenomena which, perhaps, would otherwise remain as mystery. Another important role of DNS has been the generation of reliable data that have extensively been used by turbulence modelers for preliminary assessment of their mathematical models. This has been a common practice in single-phase flows for more than a decade, and has more recently been extended to two-phase flows (see e.g. Pandya and Mashayek (2003)). These two aspects of DNS have been the primary motivation for undertaking the present study. In our previous works, we have studied the case of isothermal flows and successfully implemented the DNS data for validation of our models. In a recent work (Pandya and Mashayek, 2003), we have extended our modeling efforts to non-isothermal flows. Some of the preliminary results from the present study have already been used in Pandya and Mashayek (2003) for validation of the models derived through a probability density function (pdf) modeling approach. In the present paper, we provide the detail description of the DNS methodology and analyze the results for further physical understanding. Our analysis, however, is motivated by our greater need in the process of development and assessment of two-phase turbulence models. We will mainly focus on the evolution of various temperature statistics of both phases and their relevant contributing mechanisms. The flow configuration is that of a homogeneous shear flow superimposed by uniform mean temperature gradients in different directions. A major advantage of this configuration is that, due to its homogeneity, the entire flow field can be used for statistical analysis, thus providing highly accurate statistics.

The extent of previous DNS studies on non-isothermal two-phase flows is somewhat limited. A few studies can be found in isotropic turbulence. Jaberi (1998) showed that in the non-isothermal isotropic turbulence with stationary velocity and decaying temperature fields, the probability density function of the fluid temperature deviates farther away from a Gaussian distribution with the increase of the mass loading ratio. Jaberi and Mashayek (2000) simulated the isotropic turbulence in which both velocity and temperature fields were statistically stationary. They found that the variance of the fluid and particle temperature were increased as the mass loading ratio or the Prandtl number was increased. The mechanism of heat transfer between the two phases in the presence of a mean temperature gradient in the decaying isotropic turbulence was also investigated (Sato et al., 1998). The results showed that the particle temperature and velocity are well correlated in the direction of the mean temperature gradient.

Only a few studies have been performed on particle dispersion in turbulent homogeneous shear flows by DNS. For isothermal flows, the most recent works were performed by Ahmed and

Elghobashi (2000, 2001). The results indicated that particles modify the production rate of the turbulence kinetic energy via modifying the vorticity dynamics in cases with two-way coupling. It was also shown that for cases with one-way coupling, preferential accumulation of particles is maximum when particle time constant equals the Kolmogorov time scale. Mashayek (1998) considered both non-evaporating and evaporating droplets in compressible turbulent homogeneous shear flows. The results showed that evaporation increases both the turbulence kinetic energy and the mean internal energy of fluid by mass transfer. It was also shown that for both evaporating and non-evaporating droplets, the variances of the temperature fluctuations of both phases become independent of the initial droplet temperature after an initial transient period.

As the above brief review indicates, none of the previous studies have considered a particle-laden turbulent flow in the presence of both mean velocity and mean temperature gradients. This case is studied in the present paper. In Section 2 the problem formulation and the computational methodology are described. In Section 3 an overview of the simulations is provided. In Sections 4 and 5 the results of the simulations are presented and discussed, followed by a summary and some concluding remarks in Section 6.

2. Formulation and methodology

Numerical simulations are implemented to investigate homogeneous turbulent shear flow of an incompressible fluid (continuous phase) laden with solid particles (discrete phase). The continuous phase is a Newtonian fluid, and its instantaneous velocity, pressure and temperature are denoted by U_i, P and T, respectively. The Eulerian non-dimensional continuity, momentum and energy equations for the continuous phase are, respectively,

$$\frac{\partial U_j}{\partial x_j} = 0, \tag{1}$$

$$\frac{\partial U_i}{\partial t} + \frac{\partial}{\partial x_j}(U_i U_j) = -\frac{\partial P}{\partial x_i} + \frac{1}{Re_f}\frac{\partial^2 U_i}{\partial x_j \partial x_j} + \mathscr{S}_{ui}, \tag{2}$$

$$\frac{\partial T}{\partial t} + \frac{\partial}{\partial x_j}(U_j T) = \frac{1}{Re_f Pr}\frac{\partial^2 T}{\partial x_j \partial x_j} + \mathscr{S}_e. \tag{3}$$

In these equations, all of the variables are normalized by reference length (L_f), density (ρ_f), velocity (U_f), and temperature (T_f) scales. The reference Reynolds and Prandtl numbers are defined as $Re_f = \rho_f U_f L_f/\mu$ and $Pr = C_p\mu/\kappa$, respectively, where μ, κ, and C_p are the viscosity, the thermal conductivity, and the specific heat of the continuous phase, respectively. The length scale is conveniently chosen such that the normalized volume of the simulation box is $(2\pi)^3$, and the fluid density is used as the scale for density. The initial temperature of the fluid is the temperature scale, and the velocity scale is determined from the specified value of the reference Reynolds number. The effects of the particles on the carrier phase (i.e. the two-way coupling effects) are expressed through the terms $\mathscr{S}_{ui}$ and $\mathscr{S}_e$ which, respectively, describe the momentum and energy exchanges between the two phases. These terms and their formulation are described in Section 2.1.

The particles are assumed to be solid spheres with equal diameters smaller than the smallest length scale of the turbulence and to exhibit an empirically corrected Stokesian drag force. The

transversal motion is the only motion considered for the particles and their rotation is neglected. The density of the particles is considered to be constant and much larger than that of the fluid so that only the inertia and the drag force are significant to the particle dynamics. Gravity effects are not considered due to limitations in the numerical scheme. The particles are assumed "lumped" and each particle is at a uniform temperature. In addition, both particle–particle interaction and heat transfer due to radiation are neglected as a small volume fraction is assumed for particles. Each particle is tracked individually in a Lagrangian frame, and its instantaneous position, velocity, and temperature are denoted by X_i, V_i, and T_p, respectively. With this nomenclature, the non-dimensional Lagrangian equations describing the particle dynamics and heat transfer are (Crowe et al., 1977)

$$\frac{dX_i}{dt} = V_i, \tag{4}$$

$$\frac{dV_i}{dt} = \frac{f_1}{\tau_p}(U_i^* - V_i), \tag{5}$$

$$\frac{dT_p}{dt} = \frac{f_2}{\tau_p}(T^* - T_p), \tag{6}$$

where the superscript $*$ indicates the value of a carrier-phase variable at the particle location. The particle variables are normalized using the same reference scales used for the continuous phase variables. The non-dimensional particle time constant is $\tau_p = Re_f \rho_p d_p^2/18$, where d_p and ρ_p are the particle diameter and density, respectively.

The function $f_1 = 1 + 0.15Re_p^{0.687}$ in (5) represents an empirical correction to the Stokes drag due to particle Reynolds numbers of order unity and larger (Wallis, 1969) and is valid for particle Reynolds numbers $Re_p = Re_f \rho^* d_p |U_i^* - V_i| \leqslant 1000$. The factor $f_2 = Nu/3Pr\alpha$ represents a correlation for the convective heat transfer coefficient based on an empirically corrected Nusselt number, $Nu = 2 + 0.6Re_p^{0.5}Pr^{0.33}$ (Bird et al., 1960), where α is the ratio of the particle specific heat and the fluid specific heat.

2.1. Formulation of shear flow with mean temperature gradient

In order to configure a homogeneous shear flow for DNS, a linear mean velocity profile is applied to an initial zero-mean, random, solenoidal velocity field. Therefore, the continuous phase instantaneous velocity is $U_i = Sx_2\delta_{i1} + u_i$, in which u_i is the continuous phase fluctuating velocity. The dimensionless mean velocity gradient is defined as $S = \partial\langle U_1\rangle/\partial x_2 = \text{constant}$, where $\langle\ \rangle$ indicates the Eulerian ensemble average over the number of grid points. In this work, we also consider a mean temperature that satisfies (Blaisdell et al., 1993)

$$\frac{\partial\langle T\rangle}{\partial t} + Sx_2M_1 = 0, \tag{7}$$

where $M_i = \partial\langle T\rangle/\partial x_i$ denotes the mean temperature gradient in the x_i direction. The magnitude of M_i must be uniform in space in order to maintain a homogeneous flow, and it satisfies

$$\frac{\partial M_i}{\partial t} + S\delta_{i2}M_1 = 0, \tag{8}$$

or,

$$M_i = M_i^0 - St\delta_{i2}M_1^0, \tag{9}$$

where M_i^0 is M_i at $t = 0$. Eq. (9) states that for a mean temperature gradient initially aligned in only x_2 or x_3 directions, the mean temperature gradient is steady. However, for a mean temperature gradient initially aligned in only x_1 direction, a mean temperature gradient also develops in the x_2 direction and is time dependent. This time dependency physically arises because the fluid at large values of x_2 moves more rapidly than the fluid at small values of x_2, as a result of the shear flow (Rogers et al., 1989).

The numerical method implemented to solve the governing equations for homogeneous shear flow is the same as that of Blaisdell et al. (1993), and Rogallo (1981) and has been described in Rogers et al. (1989) in detail. A computational (deforming) coordinate system, x_i', is related to the fixed (nondeforming) system, x_i, through

$$x_i' = Q_{ij}x_j; \quad Q_{ij} = \delta_{ij} - St\delta_{i1}\delta_{j2}. \tag{10}$$

After applying the transformation to (1)–(3), and dropping the superscript $'$ on the coordinates for simplicity, the governing equations in the transformed coordinates are

$$Q_{ji}\frac{\partial u_i}{\partial x_j} = 0, \tag{11}$$

$$\frac{\partial u_i}{\partial t} + Q_{kj}\frac{\partial}{\partial x_k}(u_i u_j) = -u_2 S\delta_{i1} - Q_{ki}\frac{\partial P}{\partial x_k} + \frac{Q_{kj}Q_{lj}}{Re_f}\frac{\partial^2 u_i}{\partial x_k \partial x_l} + \mathscr{S}_{ui}, \tag{12}$$

$$\frac{\partial \theta}{\partial t} + Q_{kj}\frac{\partial}{\partial x_k}(u_j\theta) = -u_i M_i + \frac{Q_{ki}Q_{ji}}{Re_f Pr}\frac{\partial^2 \theta}{\partial x_k \partial x_j} + \mathscr{S}_e, \tag{13}$$

where $\theta = T - \langle T\rangle$ is the fluid fluctuating temperature.

By performing ensemble averaging on the particle instantaneous equations, it can be shown that the discrete phase is homogeneous within the deforming domain used to simulate the continuous phase. Because external forces and heat sources are absent, following a procedure similar to that in Barré et al. (2001), it can be shown that the mean velocity and temperature of the particles coincide with the corresponding quantities of the continuous phase, i.e. $\langle\langle V_i\rangle\rangle = \langle U_i\rangle$ and $\langle\langle T_p\rangle\rangle = \langle T\rangle$. Here, $\langle\langle\ \rangle\rangle$ denotes the Lagrangian ensemble average over the number of particles. Also, the particles are at the same initial velocities and temperatures as are their surrounding fluid elements. The particle position, fluctuating velocity and temperature in the transformed coordinates read

$$\frac{\mathrm{d}X_i}{\mathrm{d}t} = Q_{ik}v_k, \tag{14}$$

$$\frac{\mathrm{d}v_i}{\mathrm{d}t} = \frac{f_1}{\tau_p}(u_i^* - v_i) - v_2 S\delta_{i1}, \tag{15}$$

$$\frac{\mathrm{d}\theta_\mathrm{p}}{\mathrm{d}t} = \frac{f_2}{\tau_\mathrm{p}}(\theta^* - \theta_\mathrm{p}) - v_i M_i. \tag{16}$$

The source/sink terms $\mathscr{S}_{ui}$ and $\mathscr{S}_e$ appearing in (12) and (13) represent the two-way coupling effects. These Eulerian variables are calculated from the Lagrangian particle variables by volume averaging the contributions from all individual particles residing within the cell volume ($\delta\mathscr{V} = (\delta x)^3$, where δx is the node spacing) centered around each grid point. In the deforming coordinates, these terms are expressed as

$$\mathscr{S}_{ui} = -\frac{1}{\delta\mathscr{V}} \sum^{n_\mathrm{p}} \left[\frac{m_\mathrm{p} f_1}{\tau_\mathrm{p}} (u_i^* - v_i) \right], \tag{17}$$

$$\mathscr{S}_e = -\frac{1}{\delta\mathscr{V}} \sum^{n_\mathrm{p}} \left[\frac{m_\mathrm{p} f_2 \alpha}{\tau_\mathrm{p}} (\theta^* - \theta_\mathrm{p}) \right]. \tag{18}$$

In these equations, n_p is the number of particles within the cell volume and those cells with $n_\mathrm{p} = 0$ are assigned a zero value for each variable. The source term $\mathscr{S}_{ui}$ given by (17) arises because of the momentum transfer due to drag force on the particle, and the source term $\mathscr{S}_e$ given by (18) arises because of the heat transfer to/from the particle due to convection. In the derivation of (16) and (18), the heat generated by the viscous dissipation of the turbulent motions as well as that due to the particle drag are neglected.

2.2. Computational methodology and initializations

The computational methodology is the same as that employed in Mashayek and Taulbee (2002) and will not be detailed here. All of the Eulerain fields are calculated using a pseudospectral method and the Lagrangian particle equations are integrated in time using a second order accurate Adams–Bashforth method. To evaluate the continuous-phase variables at the particle location a fifth order accurate Lagrange polynomial interpolation scheme is employed. The velocity and temperature fields are initialized as random Gaussian and isotropic fields in Fourier space. The velocity field is also solenoidal. The initial spectrum, for both velocity and temperature, is calculated from $K^4 \exp[-2(K/K_s)^2]$ where K is the wave number and K_s specifies the wave number location for the peak of the energy spectrum and is chosen to be $K_s = 7$. The particles are randomly distributed in the flow at $t = 0$, with the same velocity and temperature as those of their surrounding fluid. We have considered the highest possible Reynolds number while maintaining the resolution needed for the small scales. In all simulations, $Re_f = 220$, $Pr = 0.7$, and $S = 2$. The initial values of some of the flow parameters are shown in Table 1, where Re_λ, λ, u_rms, θ_rms, ϵ, and ϵ_θ

Table 1
Flow parameters at time $t = 0$

Re_λ	63.2
λ	0.2879
u_rms	1.0
θ_rms	1.7321
ϵ	0.8405
ϵ_θ	1.4579

are, respectively, the Reynolds number based on the Taylor length scale, the Taylor length scale, the root mean square of the (isotropic) velocity fluctuation, the root mean square of temperature fluctuation, the kinetic energy dissipation rate, and the temperature fluctuation dissipation rate.

3. Overview of simulations

The number of parameters involved in the problem is too large to allow us to investigate the effects of all of them in detail. Instead, we perform a case study to compare the effects of variation of some of the parameters on the statistics of the flow and particles. The particle time constant (τ_p), the mass loading ratio (Φ_m), and the ratio of the particle and carrier phase specific heats (α) are the parameters that are considered for investigation. Table 2 shows a listing of the cases considered to study the effects of these parameters. Each of the cases shown in Table 2 are carried out with three different initial mean temperature gradients in order to observe the effects of the gradients applied in different directions. Various cases are performed in reference to a "base case" which is indicated with boldface in the table. Shown in Table 2 are also values of τ_p/τ_k (τ_k is the Kolmogorov time scale) and d_p/η (η is the Kolmogorov length scale) at times $St = 2$ and 10. For all of the cases, d_p/η varies between 0.15 and 0.3, therefore, it is reasonable to assume that the flow field around each particle is uniform. The values of τ_p/τ_k are useful in identifying the scales of the flow which are more effectively interacting with the particles (Hinze, 1972). It should be emphasized that since the governing energy equation (3) is a linear equation of the dependent variable T, the solution for any mean temperature gradient could be obtained by superposition of the solutions for M_1^0, M_2^0, and M_3^0 if we consider zero initial fluctuating temperature field. As we wish to investigate the effects of the direction of the mean temperature gradient, we simulate all cases with the same initial velocity and non-zero temperature fields. The fluctuating temperatures of continuous and discrete phases with a mean temperature gradient initially imposed in the ξ direction ($\xi = 1, 2, 3$) are denoted as θ_ξ and $\theta_{p\xi}$, respectively. All of the simulations presented here have been performed on 128^3 collocation points on a CRAY-T90 with a time step size of 2.5×10^{-3} and continued till non-dimensional time $St = 12$.

Table 2
Cases[a] considered for the study

Case reference	τ_p	Φ_m	α	Coupling	$N_p \times 10^{-5}$	τ_p/τ_k[b]	d_p/η[b]
Base case	**0.3**	**0.25**	**1**	**2-way**	**9.80**	**3.02 → 1.94**	**0.233 → 0.187**
$1.5\tau_{pb}$	0.45	0.25	1	2-way	5.32	4.53 → 2.69	0.286 → 0.220
$2\Phi_{mb}$	0.3	0.50	1	2-way	19.48	2.54 → 1.76	0.214 → 0.178
$4\alpha_b$	0.3	0.25	4	2-way	9.80	3.02 → 1.94	0.233 → 0.187
One-way	0.3	–	1	1-way	1.00	3.92 → 2.64	0.266 → 0.218

The base case is shown by boldface.

[a] Each case has been simulated for three different initial mean temperature gradients: (1) $M_1^0 = 0.2$, $M_2^0 = 0$, and $M_3^0 = 0$; (2) $M_1^0 = 0$, $M_2^0 = 2$, and $M_3^0 = 0$; (3) $M_1^0 = 0$, $M_2^0 = 0$, and $M_3^0 = 2$.

[b] Values are given at $St = 2$ and $St = 10$.

The particles are randomly distributed in the flow at $t = 0$ with the same velocity and temperature as those of their surrounding fluid. They are considered with either one- or two-way coupling with the continuous phase. The condition of one- or two-way coupling is imposed from $t = 0$ for respective cases. The total number of particles (N_p) tracked in each simulation is determined from the given values of the particle time constant and the mass loading ratio. For the one-way coupling case, the mass loading ratio is not a relevant parameter. For this case the number of particles is large enough so that the statistics do not change with the increase of the number of particles.

As has been the practice in our previous studies, before implementing the data generated by simulations for detail statistical analysis, we have made certain that various fields are sufficiently well resolved and that the assumptions invoked in the formulation of the problem are reasonably satisfied. For example, the value of ηK_{max}, where η is the Kolmogorov length scale and K_{max} is the highest wave number resolved in the simulations, was monitored throughout the simulations and was kept sufficiently larger than the acceptable limit of unity.

4. Temperature field of the continuous phase

The temporal evolution of the temperature variance of the continuous phase, $\langle\theta_\xi^2\rangle$, for the cases with initial streamwise ($\xi = 1$), cross-stream ($\xi = 2$), and spanwise ($\xi = 3$) mean temperature gradients are shown in Fig. 1a–c, respectively. As shown in the figure, an initial decay in the temperature variance is observed for all cases. After decaying to some minimum values, the temperature variance starts to grow in the later times. The growth rate of the temperature variance observed in Fig. 1a is larger than that in the other two figures. This is due to the time dependency of the mean temperature gradient for $\xi = 1$, as shown in Eq. (9). The initial decay of the temperature variance for all cases is due to the absence of the turbulent heat fluxes at $t = 0$ as will be discussed below. Another feature observed in Fig. 1 is that in spite of different directions of the mean temperature gradient for cases in Fig. 1b and c, the initial decay for $St < 2$ is very similar. This is indicative of an isotropic nature for the initial decay. An interesting feature in Fig. 1c is the appearance of some oscillations for $St \geqslant 7$. These oscillations are related to the interactions between the pressure and temperature fields which will be further discussed later in this section.

The primary effect of the particles is to decrease the temperature variance of the continuous phase comparing to the pure fluid in all times except for $St > 7$ of Fig. 1c. As indicated in Fig. 1, the one-way coupling case has the largest temperature variance among all of the cases having the same mean temperature gradients. The figure also shows that the temperature fluctuation intensity of the continuous phase decreases with increasing the mass loading, as a result of an increase of the particles effects on the fluid phase.

The effects of the change of the specific heats ratio and the particle time constant can also be noticed in Fig. 1. The increase of this ratio decreases the temperature variance of the continuous phase. As we explain later, this is due to the increase of the particle component of the temperature variance dissipation. It is observed that the decrease of the temperature variance is less significant in Fig. 1a as compared to Fig. 1b and c. The increase of the particle time constant also decreases the temperature variance because of the modifications on the turbulence heat flux.

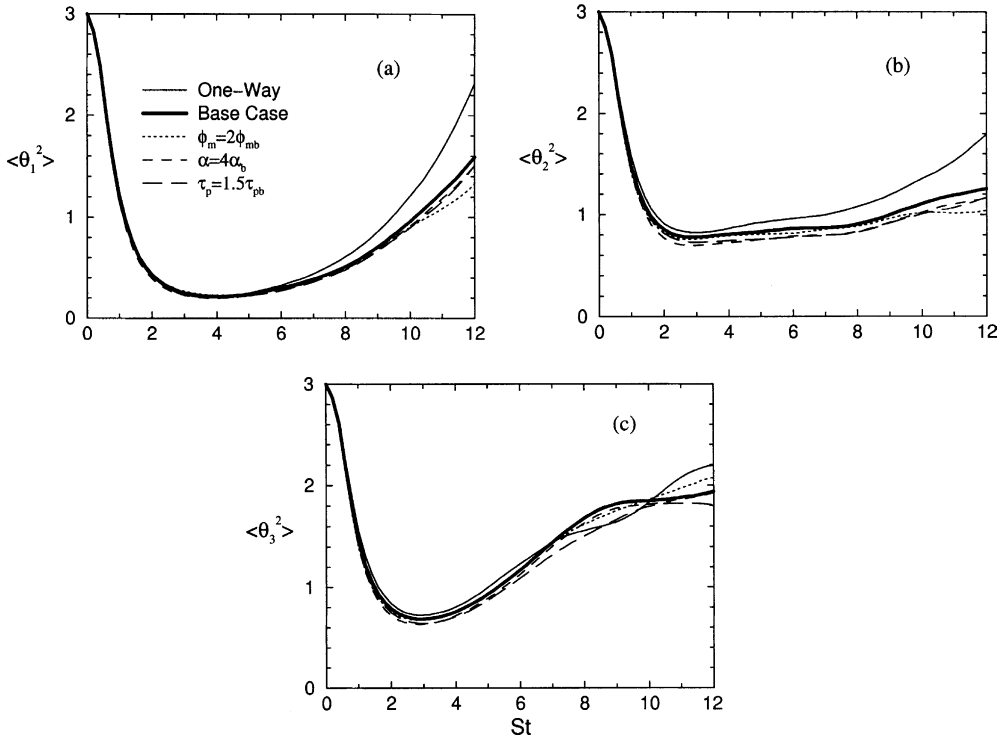

Fig. 1. Temperature variance of the fluid phase for cases with (a) initially streamwise, (b) cross-stream, and (c) spanwise mean temperature gradients.

In an attempt to explain the above observations pertaining to the evolution of the temperature variance of the continuous phase, its transport equation for a homogeneous shear flow laden with particles and in the presence of a mean temperature gradient is considered. This equation can be derived from (13) by multiplying throughout by θ and then ensemble averaging. The final form can be written as

$$\frac{\mathrm{d}\langle\theta^2\rangle}{\mathrm{d}t} = P_\theta - \epsilon_\theta + Q_\mathrm{p}, \tag{19}$$

where $P_\theta = -2\langle\theta u_i\rangle M_i$ is the production by the heat flux along with the mean temperature gradient,

$$\epsilon_\theta = \frac{2}{Re_f Pr}\left\langle \frac{\partial\theta}{\partial x_j}\frac{\partial\theta}{\partial x_j}\right\rangle \tag{20}$$

is the dissipation rate for $\langle\theta^2\rangle$ or the molecular smearing of the temperature fluctuations, and

$$Q_\mathrm{p} = -2\left\langle \frac{\alpha}{\delta\mathscr{V}}\sum^{n_\mathrm{p}}\frac{f_2 m_\mathrm{p}}{\tau_\mathrm{p}}(\theta^* - \theta_\mathrm{p})\theta^*\right\rangle, \tag{21}$$

indicates the particle contribution. The production term P_θ can be decomposed into two parts as $P_{s\theta}$ and $P_{t\theta}$, from steady and transient components of the mean temperature gradient, respectively,

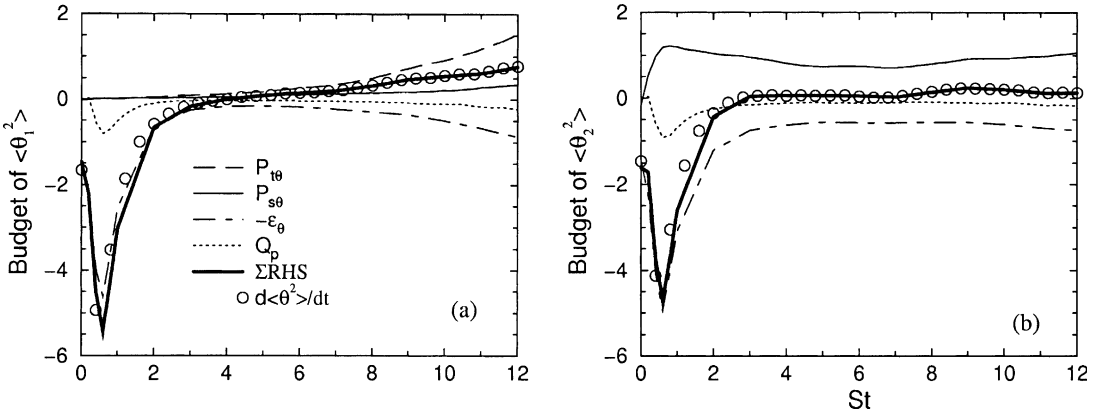

Fig. 2. Budgets of temperature variance for the base case with (a) initially streamwise and (b) cross-stream mean temperature gradients.

$$P_{s\theta} = -2\langle\theta_\xi u_\xi\rangle M^0_\xi, \quad P_{t\theta} = 2\langle\theta_1 u_2\rangle St M^0_1, \tag{22}$$

where no summation is implied over the repeated Greek indices. It is noted that $P_{t\theta}$ for the cases with cross-stream and spanwise mean temperature gradients is always zero.

The budget of the temperature variance for the base case with the initial streamwise and cross-stream mean temperature gradients is shown in Fig. 2. In this figure, $\sum RHS$ denotes the summation of all of the terms on the right-hand side of (19). The budget of the temperature variance of the base case with the spanwise mean temperature gradient is similar to that for the base case with the cross-stream mean temperature gradient and is not shown in this figure. Due to the uncorrelated initial velocity and temperature fluctuations, which results in zero turbulent heat flux, the production terms, $P_{t\theta}$ and $P_{s\theta}$, are zero at $t = 0$. In Fig. 2a, the production terms for $St < 4$, where the corresponding temperature variance is minimum according to Fig. 1a, are insignificant but in the later times $P_{t\theta}$ starts to grow fast and its difference from $P_{s\theta}$ becomes more pronounced. This difference is due to the growth of the time dependent component of the mean temperature gradient whereas the steady state component remains constant. This further explains the larger growth rate observed in Fig. 1a for temperature variance at later times. Fig. 2 also shows that ϵ_θ and Q_p both contribute to the dissipation of the temperature variance. Comparing these two terms reveals that ϵ_θ is larger than Q_p.

Now we discuss the effects of various parameters on the terms on the right-hand side of (19). In the presence of particles the production terms decrease, due to the decrease of the turbulent heat flux as explained in the next paragraph. Our results indicated that the magnitude of ϵ_θ decreases with the increase of the mass loading ratio but the magnitude of Q_p increases. Comparing ϵ_θ to Q_p always shows that ϵ_θ is more significant. On the other hand, the particles modify the fluid temperature variance mostly via modifying the turbulent heat flux as its production term, except for the case with $\alpha = 4\alpha_b$ which is modified by the modification of dissipation terms. An inspection of the energy spectra of the fluid temperature also verified that in this case modification is done mostly on the small scales rather than the larger scales of turbulence.

The temporal variation of the non-vanishing components of the turbulent heat flux $\langle\theta_\xi u_i\rangle$ are shown in Fig. 3. In the same figure, the case with $\alpha = 4\alpha_b$ gives results identical to the base case. As

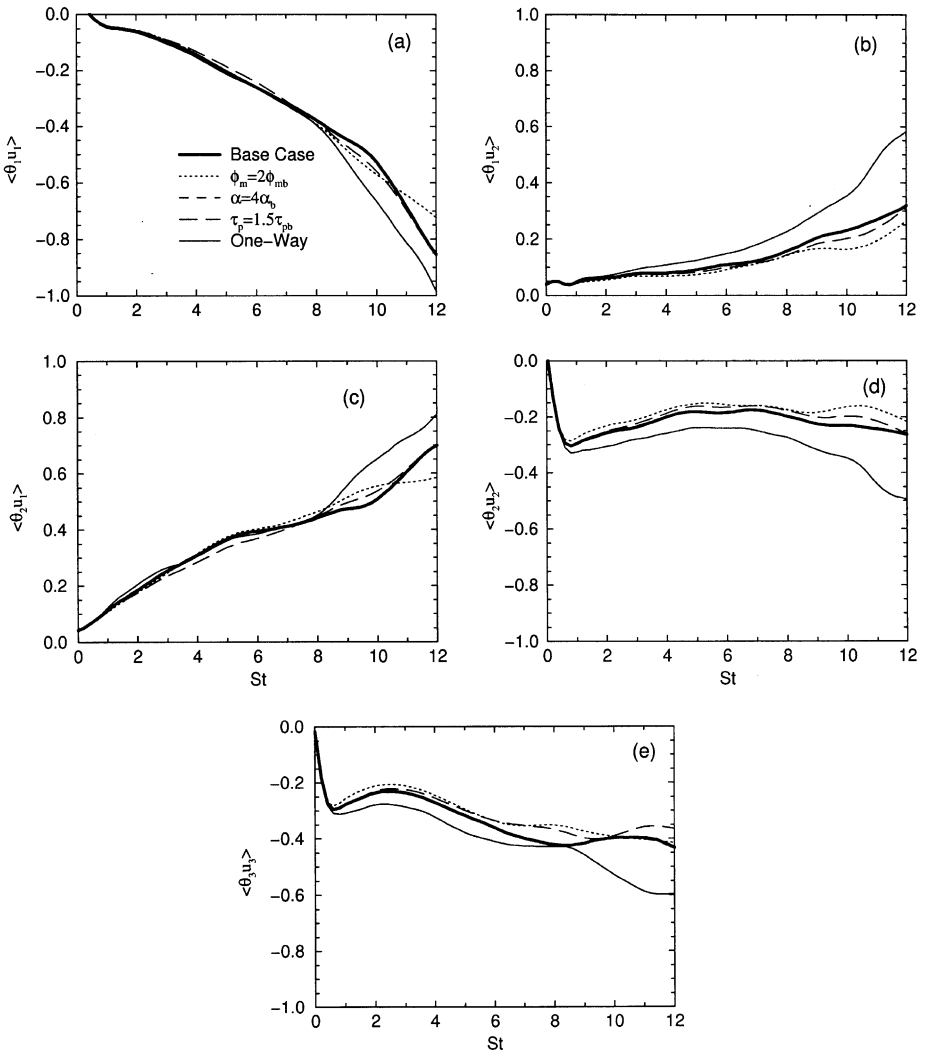

Fig. 3. Turbulent heat flux components with (a), (b) initially streamwise (c), (d) cross-stream and (e) spanwise mean temperature gradients.

the streamwise and spanwise components of the mean velocity gradient are absent, $\langle\theta_1 u_3\rangle$, $\langle\theta_2 u_3\rangle$, $\langle\theta_3 u_1\rangle$, and $\langle\theta_3 u_2\rangle$ must vanish theoretically and our DNS data also confirms that these terms are almost zero. The turbulent heat flux along with the mean temperature gradient constitutes the production term for the temperature variance according to (22). Therefore, the reasons behind many of the features observed in Fig. 1 may be found by examining Fig. 3. For example, the separation of the case with $\phi_m = 2\phi_{mb}$ at $St \simeq 10$ from the base case in Fig. 1a is due to the sudden change in the slope of $\langle\theta_1 u_2\rangle$ of the corresponding case at that time as shown in Fig. 3b. Since the heat flux magnitude of the one-way coupling case is the largest comparing to the other cases, the production term in this case results in the largest temperature variance shown in Fig. 1a and b. In general the temperature and velocity fluctuation levels decrease as a result of the two-way

coupling, so that the primary effect of the particles is to decrease the turbulent heat flux as shown in Fig. 3. In Fig. 1c, for $St > 7$ some crossing of the curves is observed which is due to the oscillatory evolution of the spanwise component of the heat flux shown in Fig. 3e. The main source of these oscillations is the correlation between the fluid pressure and its fluctuating temperature gradient, $\left\langle p\frac{\partial\theta}{\partial x_i}\right\rangle$, as discussed below.

In order to gain further insight into the evolution of the turbulent heat flux of the continuous phase, which is also one of the most important statistics from a modelling point of view, its transport equation is considered. This equation can be obtained by multiplying the momentum equation by θ and the energy equation by u_i, adding the two resulting equations, and then ensemble averaging. The final equation reads

$$\frac{\partial\langle\theta u_i\rangle}{\partial t} = -\langle u_i u_j\rangle M_j - \langle\theta u_2\rangle S\delta_{i1} + \left\langle p\frac{\partial\theta}{\partial x_i}\right\rangle - \varepsilon_{qi} + H_{pi} + M_{pi}, \tag{23}$$

where

$$\varepsilon_{qi} = \frac{1}{Re}\left(1+\frac{1}{Pr}\right)\left\langle\frac{\partial u_i}{\partial x_j}\frac{\partial\theta}{\partial x_j}\right\rangle, \tag{24}$$

$$H_{pi} = -\left\langle\frac{\alpha}{\delta\mathscr{V}}\sum^{n_\mathrm{p}}\frac{f_2 m_\mathrm{p}}{\tau_\mathrm{p}}(\theta^* u_i^* - \theta_\mathrm{p} u_i^*)\right\rangle, \tag{25}$$

$$M_{pi} = -\left\langle\frac{1}{\delta\mathscr{V}}\sum^{n_\mathrm{p}}\frac{f_1 m_\mathrm{p}}{\tau_\mathrm{p}}(\theta^* u_i^* - \theta^* v_i)\right\rangle. \tag{26}$$

The first two terms in (23) are the production terms, i.e. the Reynolds stresses along with the mean temperature gradients and the heat fluxes along with the mean strain rate. The second production term is zero for the heat flux components in the cross-stream and spanwise directions because there is no mean velocity gradient in these directions. The third term is the pressure–temperature fluctuation gradient correlation and the fourth term is due to the correlation between the gradients of fluctuating temperature and velocity of the fluid phase. The last two terms represent the contributions from the dispersed phase.

To further elaborate on the contributions of various terms in Eq. (23), the budgets of $\langle\theta_1 u_1\rangle$, $\langle\theta_2 u_2\rangle$ and $\langle\theta_3 u_3\rangle$ are considered in Fig. 4 for the base case. The two production terms, $\langle u_1 u_2\rangle M_1^0 St$ and $-\langle\theta_1 u_2\rangle S$ in Fig. 4a, both play a significant role on the temporal variation of $\langle\theta_1 u_1\rangle$ while the contribution from $-\langle u_1 u_1\rangle M_1^0$ is much smaller. This is due to the time dependency of the cross-stream component of the mean temperature gradient for this case. The modification of these production terms is, directly or indirectly, a consequence of the modification of the Reynolds stress which was discussed in our previous works (Mashayek, 1998; Mashayek and Taulbee, 2002). Our analysis of the results shows that most of the modifications of the continuous phase heat flux by particles are due to the modification of the Reynolds stress. Since the base case and the case with $\alpha = 4\alpha_\mathrm{p}$ both have the same Reynolds stress, the change of the specific heats ratio does not affect $\langle u_i u_j\rangle M_j$ as a production for the turbulent heat flux. As a result, the turbulent heat flux components for these two cases are identical in Fig. 3.

Fig. 4a also shows the contribution of the pressure term $\frac{1}{\rho}\left\langle p\frac{\partial\theta_1}{\partial x_1}\right\rangle$ and $-\varepsilon_{q1}$. Throughout the simulation time, it is observed that the magnitude of the pressure term is much larger than that of

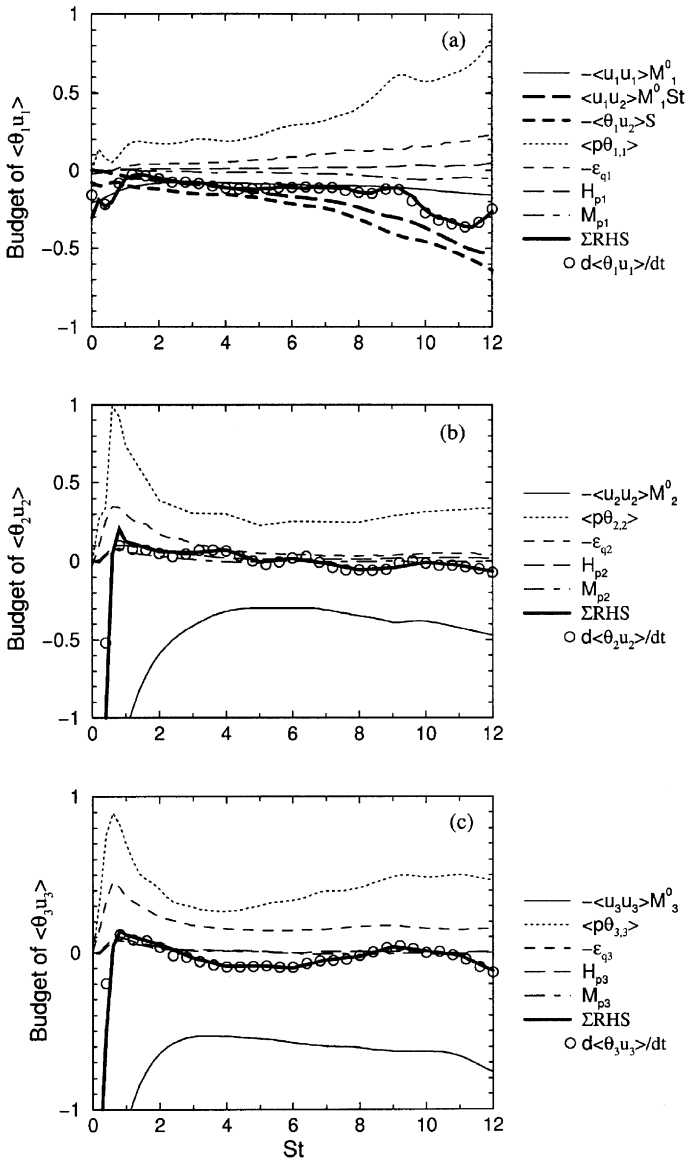

Fig. 4. Budgets of turbulent heat flux components for the base case with (a) initially streamwise (b) cross-stream and (c) spanwise mean temperature gradients.

$-\varepsilon_q$ and this domination of pressure term is also shown in Rogers et al. (1989) for the single phase flow. This figure indicates that the sudden change of $\mathrm{d}\langle\theta_1 u_1\rangle/\mathrm{d}t$ is due to the appearance of a local maximum point for the pressure term at $St \simeq 9$. In general, the observed oscillation in the temporal variation of the turbulent heat flux components in Fig. 3 is mostly due to the oscillations of the pressure term. The effect of particles on these two terms is the reduction of their magnitude and this reduction is more pronounced with the increase of the mass loading ratio. The increase of the particle time constant also decreases the magnitude of these terms but they are not sensitive to

the change of the specific heat ratio. The contribution of the particle terms H_{p1} and M_{p1} in Eq. (23) is much smaller than other terms as shown in Fig. 4 so that the modification of the heat flux is not due to these terms. The reason for this behavior will be explained in the next section which is devoted to the dispersed phase.

5. Temperature field of the discrete phase

The statistics of the particle temperature field are discussed in this section. In Fig. 5, the particle temperature variance for the cases with a cross-stream mean temperature gradient is shown. Similarly to the fluid phase, an initial decay is observed for all cases, due to the lack of an initial correlation between the temperature and velocity fields which translates into a null turbulent heat flux at $t = 0$. The heat flux, through the mean velocity gradient, is partially responsible for the production of the temperature variance. The initial decay rates of the base case, the one-way case, and the $\phi_m = 2\phi_{mb}$ case are nearly the same for $St < 2$ whereas we observe a slightly smaller rate for the $\tau_p = 1.5\tau_{pb}$ case and a much smaller rate for the case with $\alpha = 4\alpha_b$. The initial decay rate seems not to be sensitive to the change of the mass loading and observations in isotropic turbulence confirms this (Jaberi and Mashayek, 2000). It is observed that the minimum point of the temperature variance which can be considered as the end of the initial decay, is at $St \simeq 5$ for the $\alpha = 4\alpha_b$ case and at $St \simeq 3$ for other cases. During the later stages of temperature variance evolution, the growth rate in the one-way case is the largest.

To assess the relative importance of various mechanisms involved in the evolution of the particle temperature variance, the transport equation of this variance is considered.

$$\frac{\mathrm{d}\langle\langle\theta_\mathrm{p}^2\rangle\rangle}{\mathrm{d}t} = \frac{2}{\tau_\mathrm{p}}\left(\langle\langle f_2\theta^*\theta_\mathrm{p}\rangle\rangle - \langle\langle f_2\theta_\mathrm{p}^2\rangle\rangle\right) - 2\langle\langle\theta_\mathrm{p}v_i\rangle\rangle M_i, \tag{27}$$

where $\langle\langle\theta_\mathrm{p}v_i\rangle\rangle$ is the discrete phase turbulent heat flux. Our DNS results indicate that correlations of $\theta^*\theta_\mathrm{p}$ and θ_p^2 with f_2 can be approximated as $\langle\langle f_2\theta^*\theta_\mathrm{p}\rangle\rangle - \langle\langle f_2\theta_\mathrm{p}^2\rangle\rangle \cong \langle\langle f_2\rangle\rangle(\langle\langle\theta^*\theta_\mathrm{p}\rangle\rangle - \langle\langle\theta_\mathrm{p}^2\rangle\rangle)$, which is implemented in our analysis.

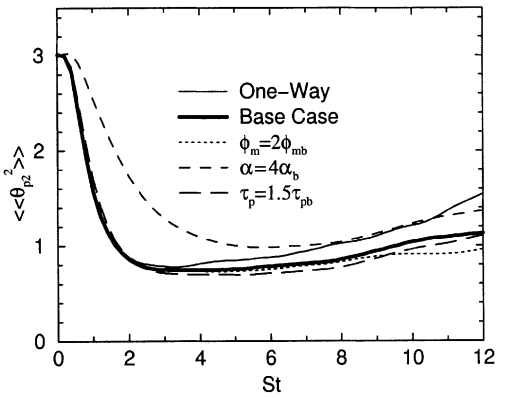

Fig. 5. Variance of particle temperature fluctuations for the cases with cross-stream mean temperature gradient.

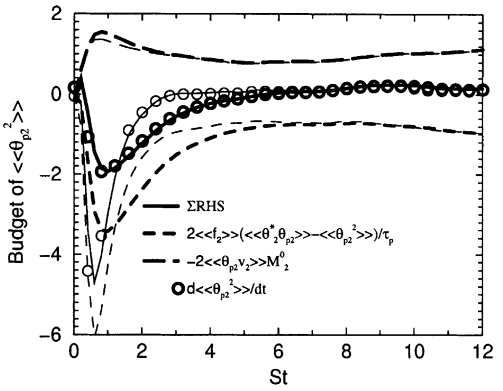

Fig. 6. Budgets of variance of particle temperature with cross-stream mean temperature gradient for the base case (thin lines) and the case with $\alpha = 4\alpha_p$ (thick lines).

With the above approximation, the contributions of different terms in Eq. (27) for the case with $\alpha = 4\alpha_b$ (thick lines) and the base case (thin lines) with a cross-stream mean temperature gradient are shown in Fig. 6. It is observed that the difference between $\mathrm{d}\langle\langle\theta_{p2}^2\rangle\rangle/\mathrm{d}t$ and ΣRHS curves is negligible for both cases, therefore, the above approximation works well here. As shown in Fig. 6, temporal evolution of the term $-2\langle\langle\theta_{p2}v_2\rangle\rangle M_2^0$ is almost the same for both cases at all times, however, temporal evolution of the first term on the right-hand side of Eq. (27) is different for times $St < 6.5$ and is again the same for the later times. Therefore, the change of α affects the rate of variation of the particle temperature variance in early times only. From a physical point of view, we can say that the increase of the particle specific heat increases the thermal response time of particles, thus the time of the particle response to the change of the surrounding fluid temperature increases.

The evolution of the ratio $(\theta_{p2})_{\mathrm{rms}}/(\theta_2^*)_{\mathrm{rms}}$ for different cases with the cross-stream temperature gradient is shown in Fig. 7. It is noted that, with the exception of the one-way case, $(\theta_{p2})_{\mathrm{rms}}/(\theta_2^*)_{\mathrm{rms}}$ is always larger than unity. This figure also indicates that the mentioned ratio is the largest for the

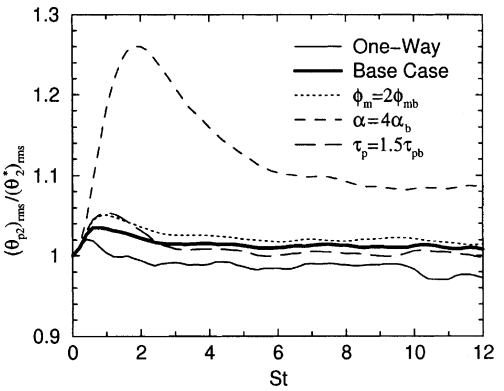

Fig. 7. Ratio of the root mean squares of particle temperature and fluid temperature at the location of particles for the cases with cross-stream mean temperature gradient.

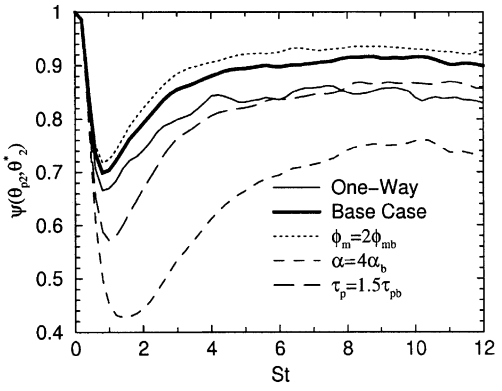

Fig. 8. Correlation factor of particle temperature and fluid temperature at the location of particles for the cases with cross-stream mean temperature gradient.

case with $\alpha = 4\alpha_b$ and the smallest for the one-way case. As shown, with an increase of the mass loading, $(\theta_{p2})_{\mathrm{rms}}/(\theta^*_2)_{\mathrm{rms}}$ increases for all of the simulation times. This suggests that the temperature fluctuation intensity of the continuous phase decreases more than the fluctuation intensity of the dispersed phase. It is also observed that with increasing the particle time constant, the ratio decreases (after $St \cong 2.5$), whereas an opposite trend exists with the increase of the particle specific heat.

In Fig. 8, the temporal evolution of θ_{p2} and θ^*_2 correlation factor, $\psi(\theta_{p2},\theta^*_2) = \langle\langle\theta_{p2}\theta^*_2\rangle\rangle \Big/ \sqrt{\langle\langle\theta^2_{p2}\rangle\rangle\langle\langle(\theta^*_2)^2\rangle\rangle}$, is presented. It appears that, after an initial rapid variation, this correlation reaches nearly stationary values at long times. These stationary values increase with increasing the mass loading ratio. Since the increase of α increases the heat capacity of all particles, the correlation factor is smaller for the $\alpha = 4\alpha_b$ case in comparison to the base case. The increase of the particle time constant also decreases the correlation factor for the same reason.

The turbulent heat flux components of the particles, $\langle\langle\theta_{p\xi}v_i\rangle\rangle$, are shown in Fig. 9. The turbulent heat flux of particles along with the mean temperature gradient, M_i, are responsible for the production of the particle temperature variance according to Eq. (27). As shown in Fig. 9, the absolute value of the heat flux components decreases with increasing the mass loading ratio. This is the primary reason for the decrease of the particle temperature variance, observed in Fig. 5, with the increase of the mass loading ratio or the particle time constant. One of the interesting features shown in Fig. 9 is that the absolute value of $\langle\langle\theta_{p2}v_2\rangle\rangle$ is not very sensitive to the increase of α whereas the absolute value of $\langle\langle\theta_{p3}v_3\rangle\rangle$ increases with the increase of α.

In order to gain further insight into the evolution of the turbulent heat flux of particles, the transport equation of this flux is considered

$$\frac{\mathrm{d}\langle\langle\theta_{\mathrm{p}}v_i\rangle\rangle}{\mathrm{d}t} = \frac{1}{\tau_{\mathrm{p}}}(\langle\langle f_2\theta^*v_i\rangle\rangle - \langle\langle f_2\theta_{\mathrm{p}}v_i\rangle\rangle) + \frac{1}{\tau_{\mathrm{p}}}(\langle\langle f_1\theta_{\mathrm{p}}u^*_i\rangle\rangle - \langle\langle f_1\theta_{\mathrm{p}}v_i\rangle\rangle) - \langle\langle v_iv_j\rangle\rangle M_j - \langle\langle\theta_{\mathrm{p}}v_2\rangle\rangle S\delta_{i1}. \tag{28}$$

Similarly to Eq. (27), here the approximations $\langle\langle f_2\theta^*v_i\rangle\rangle - \langle\langle f_2\theta_{\mathrm{p}}v_i\rangle\rangle \cong \langle\langle f_2\rangle\rangle(\langle\langle\theta^*v_i\rangle\rangle - \langle\langle\theta_{\mathrm{p}}v_i\rangle\rangle)$ and $\langle\langle f_1\theta_{\mathrm{p}}u^*_i\rangle\rangle - \langle\langle f_1\theta_{\mathrm{p}}v_i\rangle\rangle \cong \langle\langle f_1\rangle\rangle(\langle\langle\theta_{\mathrm{p}}u^*_i\rangle\rangle - \langle\langle\theta_{\mathrm{p}}v_i\rangle\rangle)$ have been invoked. The budget of

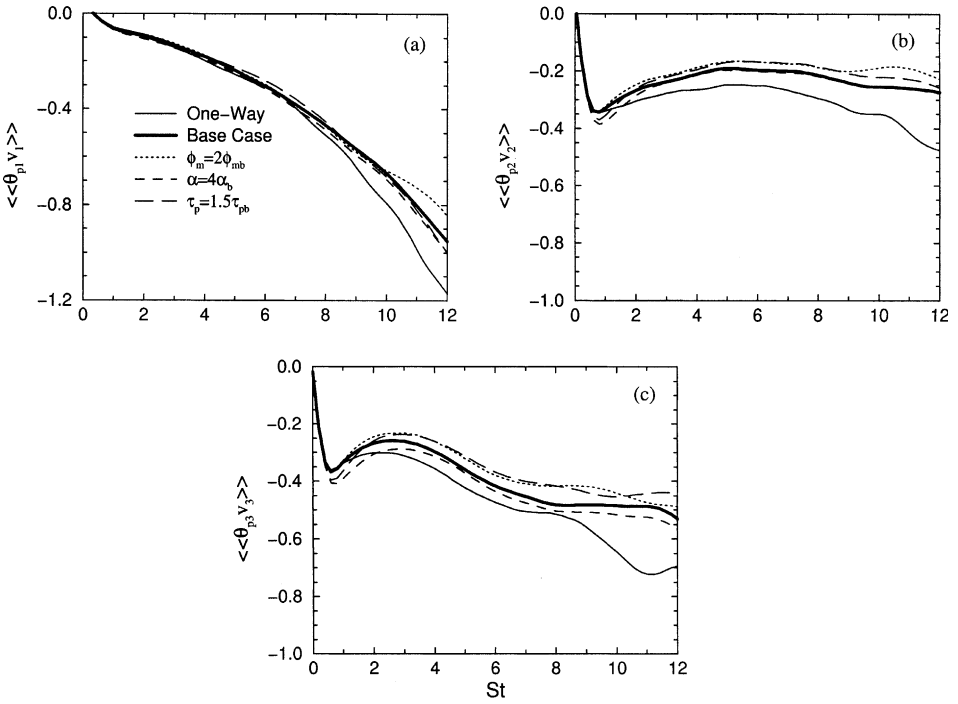

Fig. 9. Turbulent heat flux components of particles with (a) initially streamwise, (b) cross-stream and (c) spanwise mean temperature gradients.

$\langle\langle\theta_{p2}v_2\rangle\rangle$, i.e. the contributions of all non-zero terms in the right-hand side of Eq. (28), for the base case with a cross-stream mean temperature gradient is shown in Fig. 10. It is observed that the contributions from all the right-hand side terms are significant, however, the contribution of $-\langle\langle v_2v_2\rangle\rangle M_2^0$ (the third simplified term on the right-hand side of Eq. (28)) dominates in the early

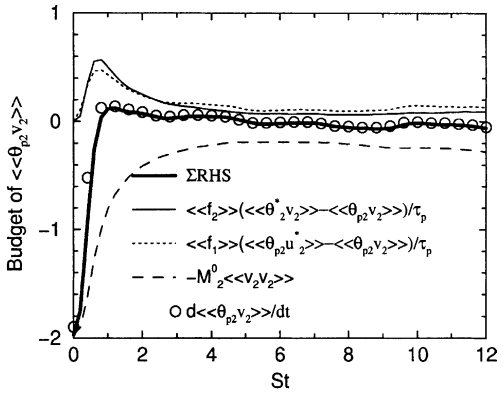

Fig. 10. Budgets of turbulent heat flux components of particles for the base case with cross-stream mean temperature gradient.

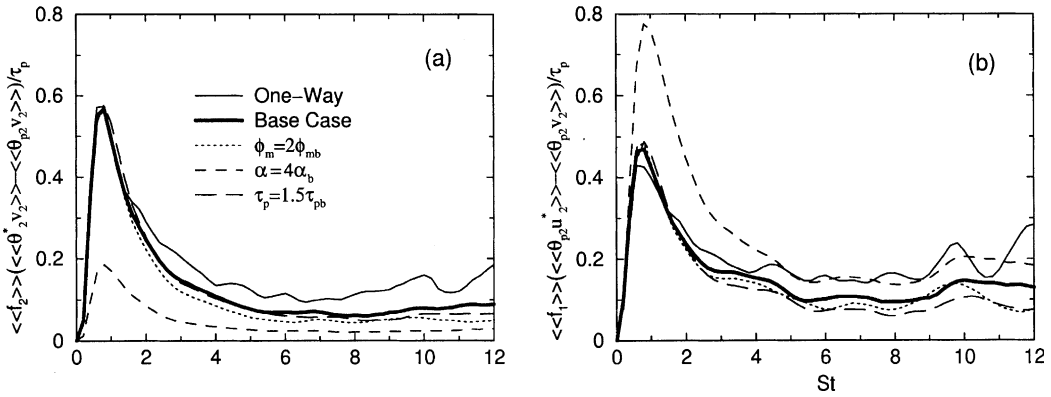

Fig. 11. Temporal variation of (a) $\langle\langle f_2\rangle\rangle(\langle\langle\theta^* v_i\rangle\rangle - \langle\langle\theta_p v_i\rangle\rangle)/\tau_p$ and (b) $\langle\langle f_1\rangle\rangle(\langle\langle\theta_p u_i^*\rangle\rangle - \langle\langle\theta_p v_i\rangle\rangle)/\tau_p$ for the base case with cross-stream mean temperature gradient.

times. As shown in our previous studies (Mashayek, 1998; Mashayek and Taulbee, 2002), the increase of the mass loading or the particle time constant results in a decrease of the magnitude of $\langle\langle v_2 v_2\rangle\rangle$ so that the effect of the change of the mass loading or the particle time constant on the turbulent heat flux of particles is carried out via the Reynolds stress of the particles. The effects of the flow parameters on the other terms on the right-hand side of Eq. (28) are discussed next.

The temporal variation of the first two terms on the right-hand side of Eq. (28) is shown in Fig. 11. As shown, the effect of the increase of the mass loading or the particle time constant is to decrease the magnitude of these terms. The increase of the particle mass loading decreases these two terms by two mechanisms. First it directly decreases the particle Reynolds number so that $\langle\langle f_1\rangle\rangle$ and $\langle\langle f_2\rangle\rangle$ decrease. Second, $(\langle\langle\theta_2^* v_2\rangle\rangle - \langle\langle\theta_{p2} v_2\rangle\rangle)$ and $(\langle\langle\theta_{p2} u_2^*\rangle\rangle - \langle\langle\theta_{p2} v_2\rangle\rangle)$ decrease with increasing the mass loading ratio. As shown in previous studies, the particle Reynolds number increases with increasing the particle time constant, therefore, $\langle\langle f_1\rangle\rangle$ and $\langle\langle f_2\rangle\rangle$ increase with the increase of τ_p. Our observation shows that $(\langle\langle\theta_2^* v_2\rangle\rangle - \langle\langle\theta_{p2} v_2\rangle\rangle)$ and $(\langle\langle\theta_{p2} u_2^*\rangle\rangle - \langle\langle\theta_{p2} v_2\rangle\rangle)$ also increase with increasing the particle time constant. Nevertheless, the overall effect of the increase of the particle time constant is to decrease the first two terms on the right-hand side of Eq. (28) due to the increase of their denominators. The comparison of the case with $\alpha = 4\alpha_b$ and the base case in Fig. 11, shows that the first term decreases and the second term increases on the right-hand side of Eq. (28) with an increase of the particle specific heat. Since all of the hydrodynamical properties of these cases are the same, the particle Reynolds numbers of the base case and the case with $\alpha = 4\alpha_b$ are the same at any time. Therefore, $\langle\langle f_1\rangle\rangle$ does not change and $\langle\langle f_2\rangle\rangle$ is multiplied by $1/\alpha$ factor. In spite of the increase of $(\langle\langle\theta_2^* v_2\rangle\rangle - \langle\langle\theta_{p2} v_2\rangle\rangle)$ with the increase of the specific heat capacity ratio, the first term of the right-hand side decreases due to the decrease of $\langle\langle f_2\rangle\rangle$. The second term on the right-hand side of Eq. (28) increases since $(\langle\langle\theta_{p2} u_2^*\rangle\rangle - \langle\langle\theta_{p2} v_2\rangle\rangle)$ increases with the increase of α.

In homogeneous shear flows with mean temperature gradients, one of the important parameters is the inclination angle of the turbulent heat flux. It has been shown in single-phase flows that, for cases with a mean temperature gradient, this angle aligns itself with the principal axis of the Reynolds stress tensor (Rogers et al., 1989). The inclination angle is defined as $\beta_f = \tan^{-1}(\langle\theta u_2\rangle/\langle\theta u_1\rangle)$ for the fluid phase, and $\beta_p = \tan^{-1}\langle\langle\theta_p v_2\rangle\rangle/\langle\langle\theta_p v_1\rangle\rangle$ for the particle phase. Fig. 12 shows the

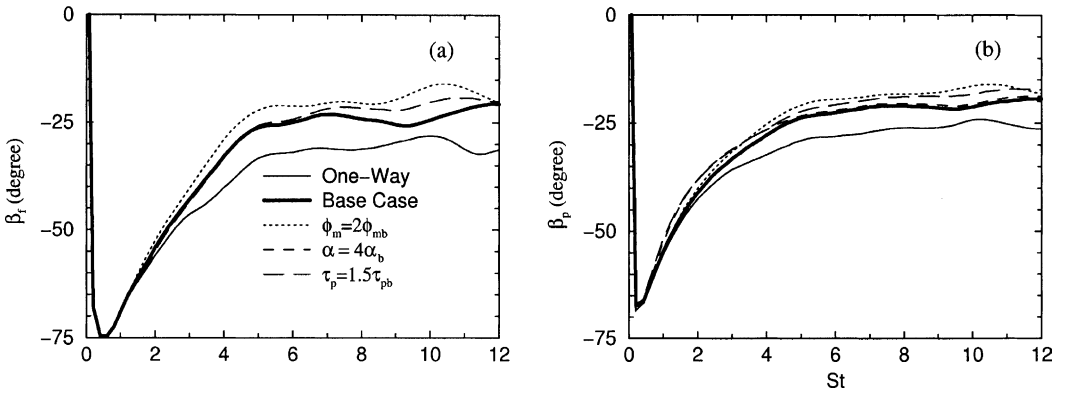

Fig. 12. Inclination angle of the turbulent heat flux of (a) the fluid phase and (b) the particle phase for the cases with cross-stream mean temperature gradient.

time evolution of β_f and β_p for cases with the cross-stream mean temperature gradient. The sudden initial increase of the magnitudes of these angles from $St = 0$ to $St \cong 0.5$ is due to the fact that the cross-stream component of the heat flux grows much faster than its stream-wise component. After $St \cong 0.5$, the magnitudes of these angles start decreasing until stationary levels are reached at long times. It is observed that the increase of the mass loading ratio or the particle time constant decreases the magnitude of the inclination angle for both phases. The increase of the ratio of specific heats does not change β_f since it does not affect the turbulent heat flux of the fluid as shown in Fig. 3.

6. Summary and concluding remarks

Direct numerical simulation is implemented to investigate the particle and fluid temperatures behavior in particle-laden homogeneous shear turbulent flows in the presence of a mean temperature gradient. Both one- and two-way couplings between the particles and the fluid are considered. The mass loading ratio, the particle time constant, the ratio of specific heats, and the orientation of the mean temperature gradient are the parameters whose influence on the particle and fluid temperature statistics are studied. The temperature variance and the turbulent heat flux, which are the primary temperature statistics in turbulent flows, are discussed in detail for both phases. Other statistics contributing to the evolution of the temperature variance and heat flux are also discussed.

The results indicate that the temperature variance and the turbulent heat flux of the fluid are decreased by the presence of the particles. The increase of either the mass loading ratio or the particle time constant generally decreases the fluid temperature variance due mostly to the decrease of the turbulent heat flux, whereas an increase of the ratio of specific heats decreases the fluid temperature variance mainly through the increase of the temperature variance dissipation terms. The ratio of specific heats is the only parameter whose influence on the fluid heat flux modification is insignificant. The increase of the mass loading ratio decreases the magnitude of the fluid turbulent heat flux. This decrease is due mainly to the modifications of the flow Reynolds

stresses. Further analysis of the cases with two-way coupling shows that the modification of the fluid temperature statistics by particles are mostly effected via the momentum coupling rather than the thermal coupling.

Various temperature statistics of the particles are also affected by the change of the above-mentioned parameters. The effect of the increase of the ratio of specific heats is to increase the temperature variance of the particles whereas that of the mass loading ratio or the particle time constant is to decrease the temperature variance of the particles. The results of our analysis also indicate that the correlation of the particle temperature and the fluid temperature at the location of the particles decreases with the increase of either the ratio of specific heats or the particle time constant. This correlation increases with the increase of the mass loading ratio. The magnitude of the particle turbulent heat flux decreases with the increase of the mass loading ratio. The heat flux magnitude increases with the increase of the ratio of the specific heats except for the cases with the cross-stream mean temperature gradient.

Acknowledgements

This work was supported in part by the National Science Foundation and the US Office of Naval Research. Computational resources for this work were in part provided by the San Diego Supercomputing Center.

References

Ahmed, A.M., Elghobashi, S., 2000. On the mechanism of modifying the structure of turbulent homogeneous shear flows by dispersed particles. Phys. Fluids 12, 2906–2930.

Ahmed, A.M., Elghobashi, S., 2001. Direct numerical simulation of particle dispersion in homogeneous turbulent shear flows. Phys. Fluids 13, 3346–3364.

Barré, C., Mashayek, F., Taulbee, D.B., 2001. Statistics in particle-laden plane strain turbulence by direct numerical simulation. Int. J. Multiphase Flow 27, 347–378.

Bird, R.B., Stewart, W.E., Lightfoot, E.N., 1960. Transport Phenomena. Wiley, New York, NY.

Blaisdell, G.A., Mansour, N.N., Reynolds, W.C., 1993. Compressibility effects on the growth and structure of homogeneous turbulent shear flow. J. Fluid Mech. 256, 443–485.

Crowe, C.T., Sharma, M.P., Stock, D.E., 1977. The Particle-Source in cell (PSI-Cell) model for gas-droplet flows. J. Fluids Eng. 6, 325–332.

Hinze, J.O., 1972. Turbulent fluid and particle interaction. In: Hetsroni, G. (Ed.), Progress in Heat and Mass Transfer, vol. 6. Pergamon Press, Oxford, pp. 433–452.

Jaberi, F.A., 1998. Temperature fluctuations in particle-laden homogeneous turbulent flows. Int. J. Heat Mass Transfer 41, 4081–4093.

Jaberi, F.A., Mashayek, F., 2000. Temperature decay in two-phase turbulent flows. Int. J. Heat Mass Transfer 43, 993–1005.

Mashayek, F., 1998. Droplet-turbulence interactions in low-Mach-number homogeneous shear two-phase flows. J. Fluid Mech. 367, 163–203.

Mashayek, F., Pandya, R.V.R., in press. Analytical description of particle/droplet-laden turbulent flows. Progress in Energy and Combustion Science.

Mashayek, F., Taulbee, D.B., 2002. Turbulent gas–solid flows. Part I: Direct simulations and Reynolds stress closures. Numer. Heat Transfer, Part B 41, 1–29.

Pandya, R.V.R., Mashayek, F., 2003. Non-isothermal dispersed phase of particles in turbulent flow. J. Fluid Mech. 475, 205–245.

Rogallo, R.S., 1981. Numerical experiments in homogeneous turbulence. NASA TM 81315.

Rogers, M.M., Mansour, N.N., Reynolds, W.C., 1989. An algebraic model for the turbulent flux of a passive scalar. J. Fluid Mech. 203, 77–101.

Sato, Y., Deutsch, E., Simonin, O., 1998. Direct numerical simulations of heat transfer by solid particles suspended in homogeneous isotropic turbulence. Int. J. Heat Fluid Flow 19, 187–192.

Wallis, G.B., 1969. One Dimensional Two Phase Flow. McGraw Hill, New York, NY.